

A NONLOCAL STRAIN MEASURE FOR DIGITAL IMAGE CORRELATION

R. B. LEHOUCQ, P. L. REU, AND D. Z. TURNER

ABSTRACT. We propose a nonlocal strain measure for use with digital image correlation (DIC). Whereas the traditional notion of compatibility (strain as the derivative of the displacement field) is problematic when the displacement field varies substantially either because of measurement noise or material irregularity, the proposed measure remains robust, well-defined and invariant under rigid body motion. Moreover, when the displacement field is smooth, the classical and nonlocal strain are in agreement. We demonstrate, via several numerical examples, the potential of this new strain measure for problems with steep gradients. We also show how the nonlocal strain provides an intrinsic mechanism for filtering high frequency content from the strain profile and so has a high signal to noise ratio. This is a convenient feature considering image noise and its impact on strain calculations.

1. INTRODUCTION

Digital image correlation has revolutionized material characterization by means of non-contact, full-field displacement measurement [1, 2, 3, 4] including several advancements towards applying DIC to characteristically difficult problems, such as extended DIC [5, 6, 7, 8, 9]. The reader is referred to the paper [10] for an overview of DIC and its applications. An important part of this process involves the mapping of displacement data with material or constitutive models via an appropriate measure of strain. There are a number of challenges to making this connection including the effects of image noise, the appropriateness of strain measures in the context of discontinuities (across pixels), and data loss from curve fitting or filtering techniques. We propose a new nonlocal strain measure that alleviates many of these issues.

Several strain measures have been proposed for DIC (for a review see [11, 12] and the reference therein). A common theme among existing strain measures involves the use of finite difference approximations of spatial partial derivatives. Although these methods have been used effectively for a variety of complex problems, there is a growing awareness of their deficiencies for problems involving cracks or strongly heterogeneous materials. Further, finite difference based approaches are sensitive to noise and often struggle to remain invariant under rigid body motion. As an alternative to these approaches, we propose a strain measure that is built on the structure of a recently proposed nonlocal vector calculus that exploits integral operators to calculate a strain.

Nonlocal vector calculus involves operators that do not use partial derivatives, but rather integrals. A comprehensive introduction to nonlocal vector calculus is given in [13] based upon preliminary work given in [14]. This formalism is applied

to a nonlocal diffusion equation in [15] and the peridynamic Navier equation [16]. In the present work, we employ these ideas to construct a robust strain measure for DIC that provides many advantages over the classical strain measure. In particular, the nonlocal strain measure intrinsically filters high frequency noise from the displacement data and is well-defined even for locations at which a classical derivative may not exist.

2. NONLOCAL STRAIN

We motivate the nonlocal strain measure by considering the one-dimensional problem. We then introduce the nonlocal strain measure for two and three dimensions. In so doing, we provide a systematic basis for computing a well-defined, discrete strain from noisy, discrete displacement data. In contrast, conventional finite difference approximations are notoriously sensitive to noisy data and inevitably lead to a tradeoff between smoothness and accuracy.

2.1. One dimension. When a function f is continuous at x , then we have the well-known relationship

$$(1a) \quad \int_{-\infty}^{\infty} f(y) \delta(y - x) dy = f(x),$$

where $\delta(x)$ is the Dirac delta (generalized) function. Probably less well-known is the relationship

$$(1b) \quad \int_{-\infty}^{\infty} f(y) \delta'(y - x) dy = -f'(x).$$

when f' is continuous at x . This is easily established by integrating by parts the lefthand side to obtain

$$\begin{aligned} \int_{-\infty}^{\infty} f(y) \delta'(y - x) dy &= f(x) \delta(x) \Big|_{-\infty}^{\infty} - \int_{-\infty}^{\infty} f'(y) \delta(y - x) dy \\ &= -f'(x), \end{aligned}$$

where we used (1a) and the formal property

$$\delta(x) = \begin{cases} 0 & x \neq 0 \\ \text{undefined} & x = 0 \end{cases}.$$

By selecting $f = 1$ in (1a) and (1b), we obtain two useful relations

$$(1c) \quad \int_{-\infty}^{\infty} \delta(y - x) dy = 1, \quad \int_{-\infty}^{\infty} \delta'(y - x) dy = 0.$$

In so many words, $\delta(x)$ and $\delta'(x)$ are even and odd functions. More generally, the former and latter functions are symmetric and antisymmetric about the origin, respectively.

The above discussion suggests a definition for the nonlocal derivative of f at x as

$$(2) \quad - \int_{-\infty}^{\infty} f(y) \alpha_{\epsilon}(y - x) dy \quad \text{where} \quad \int_{-\infty}^{\infty} \alpha_{\epsilon}(y - x) dy = 0.$$

The function α_{ϵ} is an integrable approximation to $\delta'(x)$ representing the kernel of the integral operator and the parameter ϵ is a length scale associated with the

approximation. This length scale can, for example, denote the nonzero region of compact support for α_ϵ .

The following example clarifies the procedure used to construct an appropriate α_ϵ and the role of ϵ . Consider the function

$$(3a) \quad \phi_\epsilon(x) = \begin{cases} 2 \frac{x + \gamma\epsilon}{\gamma\epsilon^2} & -\gamma\epsilon < x < 0 \\ 2 \frac{(1-\gamma)\epsilon - x}{(1-\gamma)\epsilon^2} & 0 < x < (1-\gamma)\epsilon \\ 0 & \text{otherwise} \end{cases}$$

with derivative

$$(3b) \quad \phi'_\epsilon(x) = \begin{cases} \frac{2}{\gamma\epsilon^2} & -\gamma\epsilon < x < 0 \\ -\frac{2}{(1-\gamma)\epsilon^2} & 0 < x < (1-\gamma)\epsilon \\ 0 & \text{otherwise} \end{cases}$$

where γ is a dimensionless skew parameter satisfying the constraint

$$(3c) \quad 0 < \gamma < 1.$$

A simple calculation reveals that

$$(3d) \quad \int_{-\gamma\epsilon}^{(1-\gamma)\epsilon} \phi_\epsilon(x) dx = 1, \quad \int_{-\gamma\epsilon}^{(1-\gamma)\epsilon} \phi'_\epsilon(x) dx = 0 \quad \text{for all } \epsilon > 0,$$

when γ is greater than 0 and strictly less than 1. Otherwise, the properties (3d) no longer hold. Therefore as $\epsilon \rightarrow 0$

$$(3e) \quad \begin{aligned} & \int_{-\gamma\epsilon}^{(1-\gamma)\epsilon} f(y) \phi_\epsilon(x-y) dy \rightarrow f(x) \\ & - \int_{-\gamma\epsilon}^{(1-\gamma)\epsilon} f(y) \frac{\phi'_\epsilon(x-y)}{2} dy \rightarrow f'(x), \end{aligned}$$

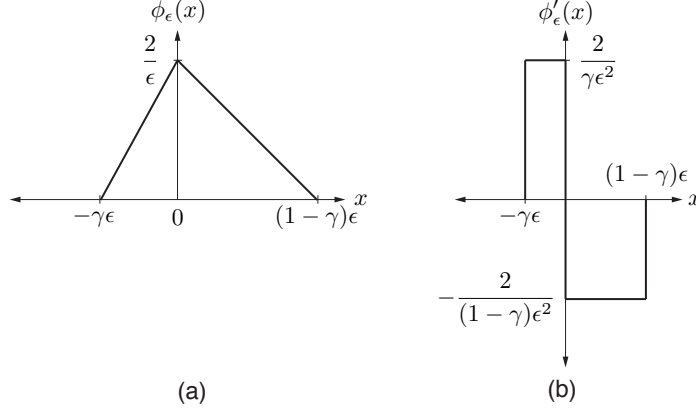
where the limits hold if f is differentiable at x . We remark that if f and ϕ_ϵ have units of length and per length, respectively, then the nonlocal derivative is a dimensionless quantity.

Plots of this kernel and its derivative are shown in Figure 1. The plots indicate that γ skews the function ϕ into the right half of the plane. This is a useful feature when x is near the end point of an interval over which approximations to $f'(x)$ are needed.

Selecting $f(x) = ax + b$ and using a midpoint quadrature rule, which is exact for linear functions, grants

$$(4) \quad \begin{aligned} & \int_{-\gamma\epsilon}^{(1-\gamma)\epsilon} (ay + b) \phi_\epsilon(x-y) dy = ax + b, \\ & - \int_{-\gamma\epsilon}^{(1-\gamma)\epsilon} (ay + b) \frac{\phi'_\epsilon(x-y)}{2} dy = a, \end{aligned}$$

so that the derivative of a linear function is computed exactly with a simple quadrature rule. Alternatively, these two relations can be established via integration by parts.

FIGURE 1. (a) Kernel function $\phi_\epsilon(x)$ and (b) its derivative.

The advantage of the nonlocal derivative is that it provides a systematic and robust basis for approximating $f'(x)$ given smooth *or irregular data*, avoiding the characteristic sensitivity of finite difference approximations to noisy data.

2.2. Two and three dimensions. Define the nonlocal gradient of a vector function \mathbf{f} as

$$(5) \quad \tilde{\nabla} \mathbf{f}(\mathbf{x}) := - \int_{\mathbb{R}^n} \mathbf{f}(\mathbf{y}) \otimes \boldsymbol{\alpha}_\epsilon(\mathbf{y} - \mathbf{x}) d\mathbf{y}$$

where $\mathbf{x} \otimes \mathbf{y}$ denotes the dyadic product of \mathbf{x} and \mathbf{y} , $\boldsymbol{\alpha}_\epsilon$ is the kernel of the integral operator approximating $\nabla \delta(\mathbf{x})$ satisfying

$$\mathbf{0} = \int_{\mathbb{R}^n} \boldsymbol{\alpha}_\epsilon(\mathbf{y} - \mathbf{x}) d\mathbf{y},$$

and $n = 1, 2, 3$ (when $n = 1$, then (2) and (5) coincide). The parameter ϵ is a length scale associated with the approximation. This length scale can, for example, denote the nonzero region of compact support for $\boldsymbol{\alpha}_\epsilon$. The nonlocal derivative (5) is a variation of the corresponding deformation gradient tensor $\bar{\mathbf{F}}$ proposed in [17, p.180] and also the weighted nonlocal gradient proposed in [13, pp.520-527]. This weighted gradient assumed that $\boldsymbol{\alpha}_\epsilon(\mathbf{y} - \mathbf{x}) + \boldsymbol{\alpha}_\epsilon(\mathbf{x} - \mathbf{y}) = \mathbf{0}$, a sufficient, but not necessary, condition to satisfy the second integral in (5). As discussed in the one-dimensional case, if \mathbf{f} and $\boldsymbol{\alpha}_\epsilon$ have units of length and per volume per length, then the nonlocal gradient is a dimensionless quantity.

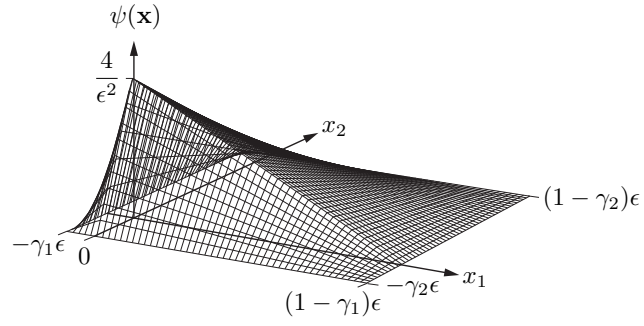
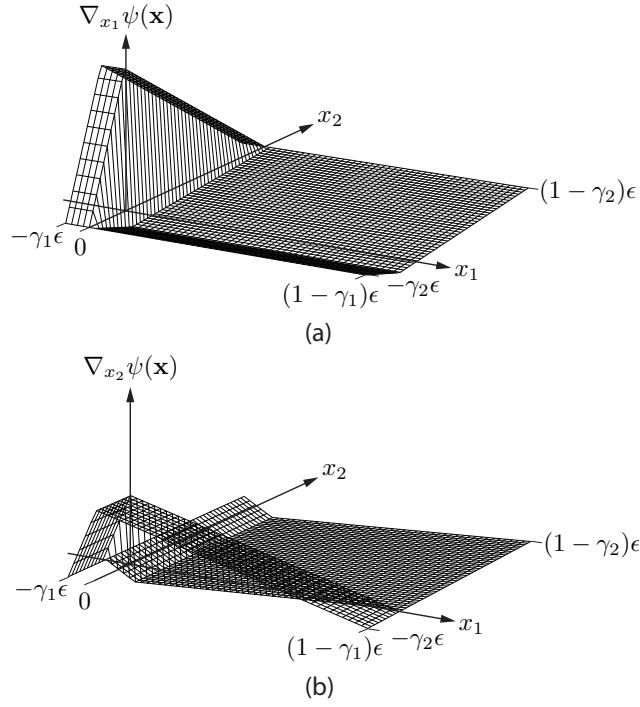
The determination of an appropriate $\boldsymbol{\alpha}_\epsilon$ follows as in the one-dimensional case. As an example, let the scalar function

$$\psi(\mathbf{x}) = \psi(x_1, x_2) = \phi_{1,\epsilon}(x_1) \phi_{2,\epsilon}(x_2),$$

where $\phi_{1,\epsilon}, \phi_{2,\epsilon}$ are the one-dimensional functions given by (3) with skew parameters $0 < \gamma_1 < 1$, and $0 < \gamma_2 < 1$, respectively (see Figure 2). Therefore

$$\boldsymbol{\alpha}_\epsilon(\mathbf{x}) = \nabla \psi(\mathbf{x}) = \left(\frac{\partial \phi_{1,\epsilon}(x_1)}{\partial x_1} \phi_{2,\epsilon}(x_2), \frac{\partial \phi_{2,\epsilon}(x_2)}{\partial x_2} \phi_{1,\epsilon}(x_1) \right).$$

A plot of the components of $\boldsymbol{\alpha}_\epsilon(\mathbf{x})$ is shown in Figure 3. By construction, we see

FIGURE 2. Plot of $\psi(\mathbf{x})$.FIGURE 3. Plot of the components of $\alpha_\epsilon(\mathbf{x})$, (a) $\nabla_{x_1}\psi(\mathbf{x})$ (b) $\nabla_{x_2}\psi(\mathbf{x})$

that

$$\int_{\mathbb{R}^2} \psi(\mathbf{x}) \, d\mathbf{x} = 1, \text{ and } \int_{\mathbb{R}^2} \nabla \psi(\mathbf{x}) \, d\mathbf{x} = \mathbf{0}.$$

2.3. Homogenous deformation. Selecting the function $\mathbf{f} = \mathbf{A} \mathbf{x} + \mathbf{c}$, where \mathbf{A} and \mathbf{c} are a constant tensor and vector, results in

$$\begin{aligned}
\tilde{\nabla}(\mathbf{A} \mathbf{x} + \mathbf{c}) &= \tilde{\nabla} \mathbf{A} \mathbf{x} + \tilde{\nabla} \mathbf{c} \\
&= -\mathbf{A} \int_{\mathbb{R}^2} \mathbf{y} \otimes \boldsymbol{\alpha}_\epsilon(\mathbf{y} - \mathbf{x}) \, d\mathbf{y} + \mathbf{c} \otimes \int_{\mathbb{R}^2} \boldsymbol{\alpha}_\epsilon(\mathbf{y} - \mathbf{x}) \, d\mathbf{y} \\
&= -\mathbf{A} \int_{\mathbb{R}} \int_{\mathbb{R}} (y_1, y_2) \\
&\quad \otimes \left(\frac{\partial \phi_{1,\epsilon}(y_1 - x_1)}{\partial y_1} \phi_{2,\epsilon}(y_2 - x_2), \frac{\partial \phi_{2,\epsilon}(y_2 - x_2)}{\partial y_2} \phi_{1,\epsilon}(y_1 - x_1) \right) \\
&\quad dy_1 dy_2 \\
&= -\mathbf{A}(-\mathbf{I}) = \mathbf{A},
\end{aligned}$$

where \mathbf{I} denotes the unit tensor and the fourth equality follows from integrating by parts each of the four components of the tensor.

In particular, the above derivation demonstrates that

$$(6) \quad \tilde{\nabla}(\mathbf{A} \mathbf{x}) = \mathbf{A} \tilde{\nabla} \mathbf{x} = \mathbf{A},$$

so that $\tilde{\nabla}$ commutes with a constant tensor exactly as does the classical gradient operator. Moreover, when $\mathbf{A} = \mathbf{I}$ then $\tilde{\nabla} \mathbf{x} = \mathbf{I}$, or in words, the nonlocal gradient of the identity vector map is the identity tensor.

2.4. Definition of nonlocal strain. Consider the nonlocal deformation gradient defined as

$$(7a) \quad \tilde{\mathbf{F}} := \mathbf{I} + \tilde{\nabla} \mathbf{u}.$$

The nonlocal strain tensor, $\tilde{\mathbf{E}}$, is then defined as

$$(7b) \quad \tilde{\mathbf{E}} := \frac{1}{2}(\tilde{\mathbf{F}}^T \tilde{\mathbf{F}} - \mathbf{I}).$$

2.5. Rigid body motions and finite rotations. For this nonlocal strain measure to be of meaningful value, the property $\tilde{\mathbf{F}}^T \tilde{\mathbf{F}} = \mathbf{I}$ must hold for any motion that does not deform the body. In other words, the nonlocal strain should be invariant under rigid body motion defined by the mapping

$$(8a) \quad \zeta(\mathbf{x}) = \mathbf{R} \mathbf{x} + \mathbf{c}$$

with rigid body displacement

$$(8b) \quad \mathbf{u}_{rb}(\mathbf{x}) := \zeta(\mathbf{x}) - \mathbf{x} = (\mathbf{R} - \mathbf{I}) \mathbf{x} + \mathbf{c},$$

where \mathbf{R} is a rotation tensor, i.e., $\mathbf{R}^T \mathbf{R} = \mathbf{I}$ with positive determinant, and \mathbf{c} is a constant vector. The corresponding nonlocal deformation gradient is

$$(8c) \quad \mathbf{I} + \tilde{\nabla} \mathbf{u}_{rb} = \mathbf{I} + (\mathbf{R} - \mathbf{I}) = \mathbf{R},$$

where we used (6) for the first equality so that

$$(\mathbf{I} + \tilde{\nabla} \mathbf{u}_{rb})^T (\mathbf{I} + \tilde{\nabla} \mathbf{u}_{rb}) = \mathbf{I}$$

as required for the nonlocal strain to be invariant under rigid body motion.

2.6. Nonlocal strain over a bounded domain. Let Ω represent a bounded open domain partitioned into M non-overlapping subdomains Ω_i with boundary Γ such that

$$(9) \quad \Omega = \bigcup_{i=1}^M \Omega_i .$$

In the context of DIC, Ω_i represents the decomposition of data as either pixels or collections of pixels with an associated area.

Let \mathbf{u}_i denote the displacement over Ω_i . Since the value of \mathbf{u}_i is constant over Ω_i , the displacement vector field over Ω is

$$(10) \quad \mathbf{u}(\mathbf{x}) = \sum_{j=1}^M \mathbf{u}_j \mathbb{1}_{\Omega_j}(\mathbf{x})$$

where the indicator function $\mathbb{1}_{\Omega_j}$ is given by

$$\mathbb{1}_{\Omega_j}(\mathbf{x}) := \begin{cases} 1 & \mathbf{x} \in \Omega_j , \\ 0 & \mathbf{x} \notin \Omega_j . \end{cases}$$

Inserting the DIC displacement (10) into (5) results in

$$(11a) \quad \tilde{\nabla} \mathbf{u}(\mathbf{x}) = - \sum_{j=1}^M \mathbf{u}_j \otimes \int_{\Omega_j} \nabla \psi(\mathbf{y} - \mathbf{x}) \, d\mathbf{y} \quad \mathbf{x} \in \Omega ,$$

or equivalently,

$$(11b) \quad \tilde{\nabla} \mathbf{u} = - \sum_{j=1}^M \mathbf{u}_j \otimes \tilde{\nabla} \mathbb{1}_{\Omega_j} \text{ over } \Omega .$$

These two relations explain that the function $\nabla \psi(\mathbf{x})$ need not be evaluated directly, but rather only its integral over the subdomain Ω_j is needed. This is an important result, given that $\nabla \psi(\mathbf{x})$ is not defined at the origin or along the axes.

A special case occurs when $\mathbf{c} = \mathbf{u}_1 = \mathbf{u}_2 = \dots = \mathbf{u}_M$ so that $\mathbf{u}(\mathbf{x}) = \mathbf{c} \mathbb{1}_{\Omega}(\mathbf{x})$ and

$$\tilde{\nabla}(\mathbf{c} \mathbb{1}_{\Omega}) = \mathbf{c} \tilde{\nabla} \mathbb{1}_{\Omega} .$$

If we suppose that Ω is a region such that for any $\mathbf{x} \in \Omega$, there exists skew parameters γ_1 and γ_2 that satisfy the constraint (3c) (the support of $\psi(\mathbf{x})$ is contained within Ω) then

$$\tilde{\nabla} \mathbb{1}_{\Omega}(\mathbf{x}) \equiv \mathbf{0} \quad \mathbf{x} \in \Omega .$$

For example, if Ω is a rectangle, then the above conditions can be fulfilled since either γ_1 or γ_2 (or both) can be selected appropriately when \mathbf{x} is close to the boundary, Γ , of Ω .

2.7. Discrete approximation. The invariance under rigid body motion for the discrete approximation to $\tilde{\mathbf{E}}$ also holds assuming a sufficiently accurate quadrature rule is used to integrate $\nabla \psi$ and \mathbf{u} . This can be easily verified. Consider a square, two-dimensional domain of size $L \times L$, where $L = 100$ units, with a synthetic rigid body displacement field of the form

$$(12) \quad \mathbf{R} = \begin{bmatrix} \cos \theta & -\sin \theta \\ \sin \theta & \cos \theta \end{bmatrix} , \quad \mathbf{c} = \mathbf{0} ,$$

where $\theta = 45$ degrees. The domain is discretized into cells (pixels) of size one unit \times one unit. Computing the nonlocal strain according to (7b) for various values of ϵ results in the strain values given in Table 1, which shows that the strain is indeed negligible.

TABLE 1. L_2 -norms of the nonlocal strain for various support sizes

ϵ	$\bar{\mathbf{E}}_{11}$	$\bar{\mathbf{E}}_{12}$	$\bar{\mathbf{E}}_{21}$	$\bar{\mathbf{E}}_{22}$
10	5.9e-15	6.9e-15	6.9e-15	1.1e-14
8	5.3e-15	6.7e-15	6.7e-15	1.2e-14
6	7.0e-15	9.1e-15	9.1e-15	1.7e-14
4	9.9e-15	1.0e-14	1.0e-14	1.8e-14
2	2.0e-14	2.0e-14	2.0e-14	2.7e-14

As an aside, when the displacement is given by (10), care needs to be taken to align the discontinuity of $\nabla\psi$ over the pixel containing the origin with a pixel boundary for the quadrature involving $\nabla\psi$ since by (11) the displacement is constant over Ω_j . We also remark that the nonlocal strain at a point depends upon all the values of the displacement field surrounding the point. The quadrature for the discrete approximation of the nonlocal strain is akin to using an extremely high order differencing scheme, except that the stencil is over the full area of the nonlocal support, not just along the coordinate directions aligned with the positive and negative x_1 and x_2 axes (as it is in finite difference difference approximations to the classical gradient).

2.8. Virtual strain gauge. For the purpose of comparison, we include here a brief description of how strain is typically calculated in the context of DIC. There are a number of nuances related to the various methods available, but in general, they fall into two categories: those that apply finite differencing to the displacement data and those that use polynomial smoothing. In either case, filtering may also be applied. In the case of local polynomial smoothing, a polynomial function is fit to the displacement data over a particular region. This region is defined by the strain window size, which can be considered as a regularization parameter for a given polynomial basis. It can be shown that this process effectively acts as a low pass filter. The resulting strain measure is highly sensitive to the virtual strain gauge (VSG) size (and the subset size), where the VSG size is a function of the strain window and step size. For small VSG sizes, the resulting strain field will be more accurate, but contain a large amount of noise. Conversely, a large VSG size limits the amount of noise, but tends towards less accuracy. In the numerical examples below, we perform a comparison between the VSG approach and the nonlocal strain measure to illustrate the differences between the two.

3. NUMERICAL RESULTS

In this section we demonstrate the performance of the nonlocal strain for a number of examples including verification problems and results for images taken from experiments.

3.1. Non-fully-differentiable function on a bounded domain. The nonlocal strain, as detailed in §2.4, is well defined within the domain including at pixel interfaces and for fields that are continuous but not differentiable. To illustrate these two features, consider a square domain of size $L \times L$ units with a displacement profile of the form

$$(13) \quad \begin{aligned} u_1(\mathbf{x}) &= \begin{cases} x_1 & 0 < x_1 \leq L/2 \\ L - x_1 & L/2 < x_1 < L \end{cases} \\ u_2(\mathbf{x}) &= \begin{cases} x_2 & 0 < x_2 \leq L/2 \\ L - x_2 & L/2 < x_2 < L \end{cases} \end{aligned}$$

Note that $\mathbf{u}(\mathbf{x})$ is not differentiable along the lines $x_1 = L/2$ and $x_2 = L/2$. The displacement profile is shown in Figure 4. The four components of the nonlocal strain tensor are shown in Figure 5. The nonlocal strain does not suffer from boundary effects if the support of α_ϵ is weighted properly towards the interior of the domain using the skew parameters γ_1 and γ_2 . It is also important to point out that in this example the discontinuity lies on the interface between two subdomains Ω_j .

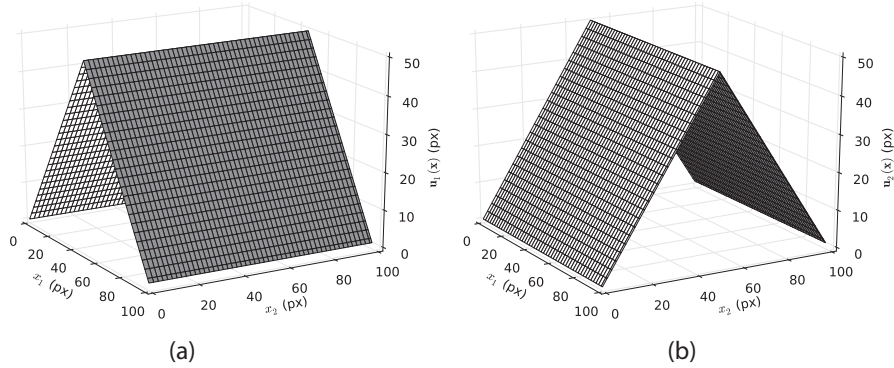


FIGURE 4. (a) Non-fully-differentiable displacement data $u_1(\mathbf{x})$
(b) $u_2(\mathbf{x})$

3.2. Nonlocal strain and noisy data. This numerical example demonstrates the effectiveness of the nonlocal strain measure for noisy data. The vector displacement profile for this example was generated by adding noise (with mean 0 and standard deviation 5%) to a smooth function over a square domain of size 100 by 100 pixels. The displacement profile is given as

$$(14) \quad \begin{aligned} u_1(\mathbf{x}) &= \sin\left(\frac{a}{2\pi}x\right) \cos\left(\frac{a}{2\pi}y\right) + \sigma_{n1} \\ u_2(\mathbf{x}) &= \cos\left(\frac{a}{2\pi}x\right) \sin\left(\frac{a}{2\pi}y\right) + \sigma_{n2}, \end{aligned}$$

where $a = 1/5$ and σ_n is the amount of noise. Figure 6 shows the noisy displacements plotted over the domain. For the purpose of comparison, Figure 7 shows the nonlocal strain component $\bar{\mathbf{E}}_{11}$ computed for the noisy displacement data vs. the

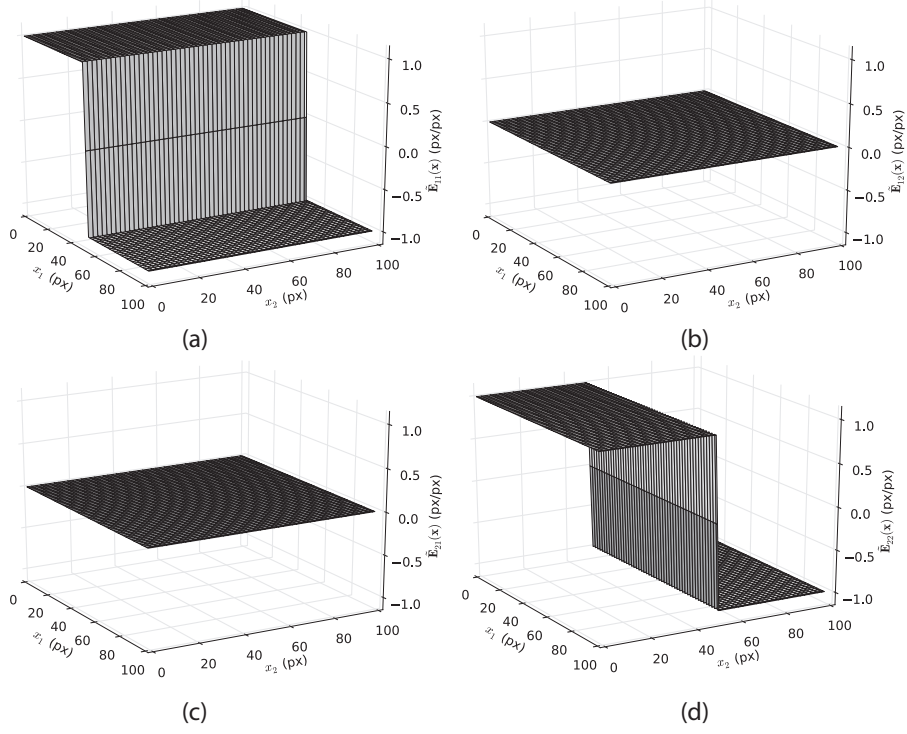


FIGURE 5. Components of the nonlocal strain tensor applied to the non-fully-differentiable displacement field (a) $\tilde{\mathbf{E}}_{11}$ (b) $\tilde{\mathbf{E}}_{12}$ (c) $\tilde{\mathbf{E}}_{21}$ (d) $\tilde{\mathbf{E}}_{22}$

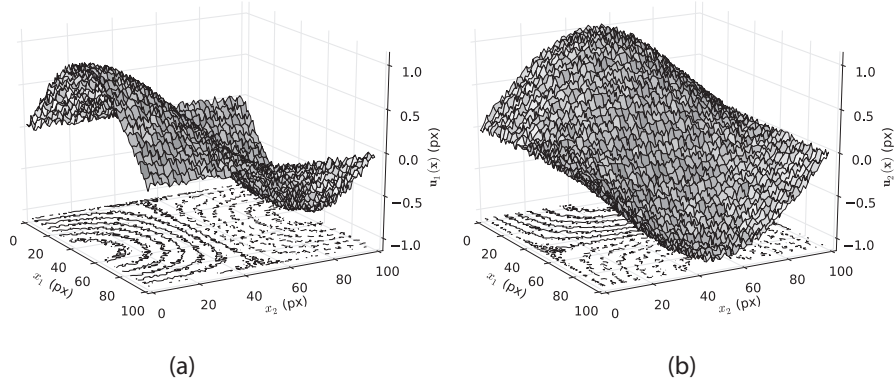


FIGURE 6. (a) Noisy displacement data $u_1(\mathbf{x})$ (b) $u_2(\mathbf{x})$

classical strain component \mathbf{E}_{11} for the vector field (14) with the noise suppressed, i.e., $\sigma_{n1} = \sigma_{n2} = 0$.

The nonlocal strain was computed using a support size, $\epsilon = 20$ units. This example demonstrates the robustness of the nonlocal strain measure in the context

of noisy data and that the nonlocal strain is in agreement with the classical strain. Similar results hold for the other nonlocal strain components, although not shown here. The error in each component of the nonlocal strain is shown in Figure 8.

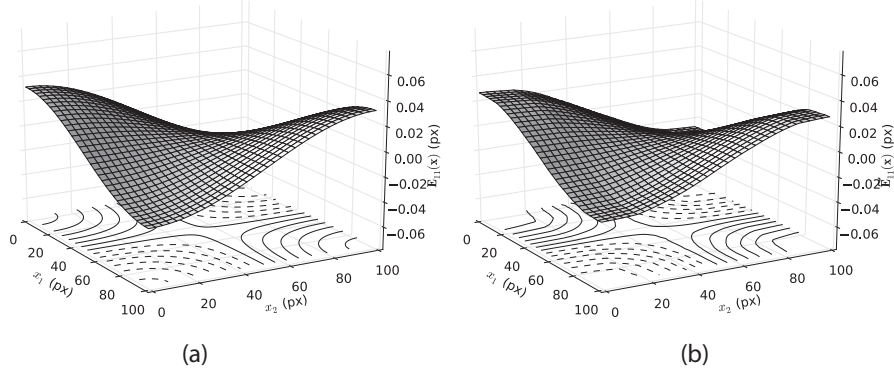


FIGURE 7. (a) Classical strain component \mathbf{E}_{11} computed by taking the derivative of the displacement profile with no noise (b) nonlocal strain component $\tilde{\mathbf{E}}_{11}$ computed for the noisy displacement profile.

3.3. DIC Challenge: synthetic strain concentrations of various periods and amplitudes. This example shows the nonlocal strain measure as applied to one of the DIC Challenge [18] image sets with synthetic pixel displacements applied to induce strain concentrations of various periods and amplitudes. The data used in this example represent Sample 15 from the DIC Challenge images. The details of how the images were constructed are given on the DIC Challenge website. The reference image is `Ref.tif` and the deformed image is `P200_K50.tif`. The correlation parameters used are given in Table 2. A step size of one pixel was used to enable evaluating the VSG and nonlocal strain measures with small support or small strain window size. It should be pointed out that the subset solutions are not independent at this step size [19].

The displacement profile for a vertical line drawn through the images at $x = 1000$ pixels is shown in Figure 9. Figure 10 shows the nonlocal strain results for this data set for various values of ϵ compared to the VSG method with various strain window sizes. To compute the VSG results, the Ncorr [20] software was used.

As expected, for larger values of ϵ the high frequency content of the nonlocal strain measure is effectively filtered out, but note the overall structure of the strain profile is preserved (multiple sub-peaks in the main strain concentration are captured). Using a larger strain window size also smooths the result, but the structure is not preserved. Reported in Figure 10 is the maximum strain computed for each method, for each nonlocal support or strain window size. Taking the single pixel nonlocal support value of the maximum strain as the most accurate, the loss in accuracy going to a support size of 20 pixels is 9.4%, whereas the loss in accuracy of the VSG method is 17.0%, suggesting that smoothing the strain data with the VSG method leads to greater loss in accuracy than using the nonlocal strain.

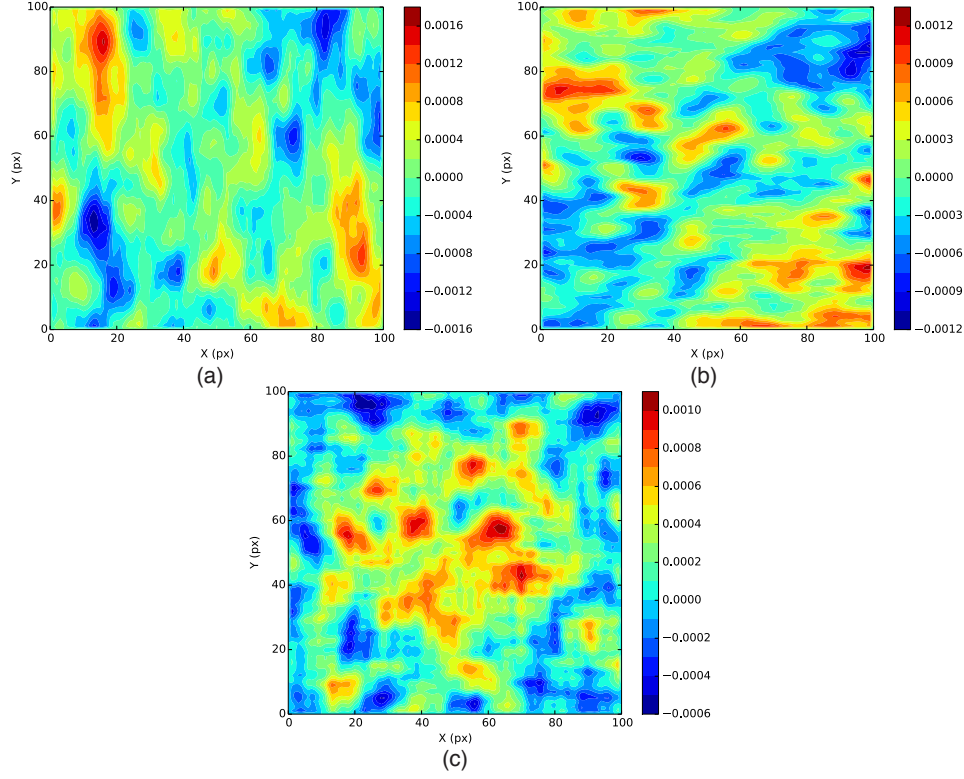


FIGURE 8. Error in the nonlocal strain components (a) $\tilde{\mathbf{E}}_{11}$ (b) $\tilde{\mathbf{E}}_{22}$ (c) $\tilde{\mathbf{E}}_{12}$.

TABLE 2. Correlation parameters used for Sample 15 images

Parameter	Value
Subset size	25
Step size	1
Interpolation	Bicubic
Matching criterion	SSD
Virtual strain gauge size	Varies from 1 to 20
Test function support, ϵ_1 or ϵ_2	Varies from 1 to 20

3.4. DIC Challenge: experimental data for a plate with a hole being loaded in tension. This example involves computing the nonlocal strain from images taken of a steel plate with a small hole being loaded in tension. The images were obtained from the DIC Challenge website and represent Sample 12. Table 3 lists the parameters used in the correlation to obtain the displacement values. Note that a step size of one was chosen to introduce the maximum amount of high frequency content into the displacement solution. It is well known that increasing the step size leads to a smoother strain profile, but decreases accuracy as it introduces artificial dissipation of the displacement gradients. Using a virtual strain gauge approach to calculate the strain inevitably leads to a tradeoff between accuracy

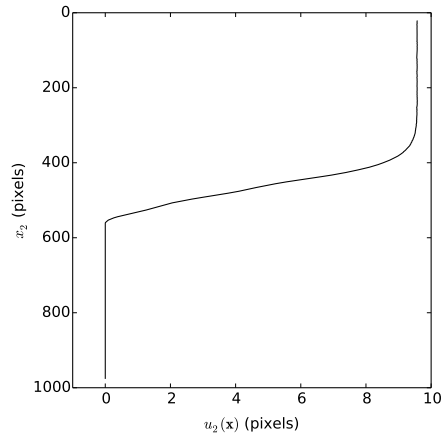


FIGURE 9. Displacement profile of the DIC Challenge, Sample 15 data set for a vertical line drawn through the images at $x = 1000$ pixels.

TABLE 3. Correlation parameters for the plate with a hole images

Parameter	Value
Subset size	35
Step size	1
Interpolation	Bilinear
Matching criterion	SSD
Test function support, ϵ_1 or ϵ_2	Varies from 5 to 50 pixels

and smoothness. Large strain gradients cannot be captured if too much smoothing is introduced, leading to poor accuracy. Conversely, resolving steep gradients leads to a highly oscillatory solution.

Figure 11 shows the strain calculated using equation (7b) with the test function of equation (3) for varying sizes of the test function support, ϵ . It can be seen from Figure 11 that ϵ acts as a filter for high frequency content, but does not introduce dissipation, leading to a *smooth and accurate strain profile*.

4. CONCLUSIONS

We have introduced a new, nonlocal measure of strain for use in digital image correlation that is both noise filtering and appropriate for discontinuous displacement fields. With regard to noise, as opposed to curve fitting processes that discard data, the nonlocal process incorporates the full data set, but diminishes the effect of outliers by a distributed weighting of values that has a smoothing effect. In this way, the nonlocal strain maintains high fidelity data content without oscillations. Another feature of the nonlocal strain measure is that it gives the same result as the classical strain measure for differentiable displacement fields, but also provides a meaningful value when the displacement field is discontinuous (in which case the classical strain is not defined). We have also shown that this strain measure is invariant under rigid body motion, which is necessary to prevent non-physical strains

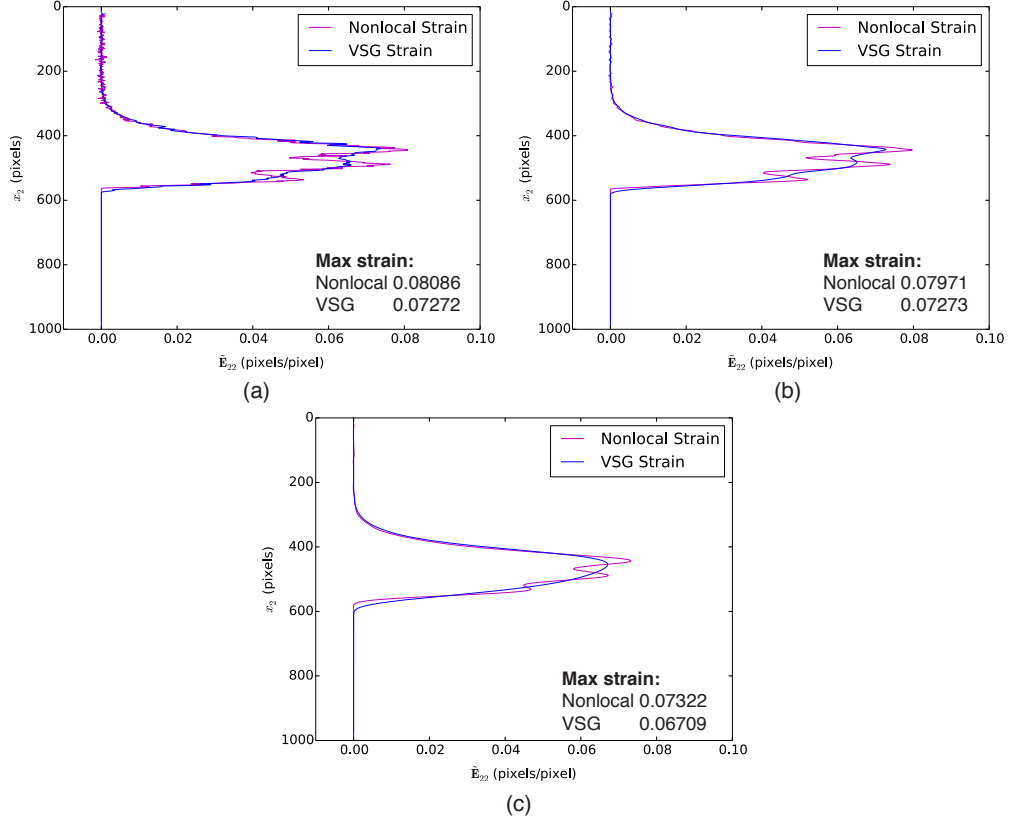


FIGURE 10. Nonlocal strain calculated for the DIC Challenge, Sample 15 images. (a) $\epsilon = 1$ pixel, strain window size = 1 (b) $\epsilon = 5$ pixels, strain window size = 5 (c) $\epsilon = 20$ pixels, strain window size = 20.

from arising due to large rotations or motion without deformation. Through a number of academic and experiment-based numerical examples we have demonstrated the effectiveness of this strain measure for both problems with analytic solutions and problems of engineering relevance. The results reveal that the nonlocal strain measure provides smoothing with less loss of accuracy than the VSG method. Ultimately, this work provides a framework to connect material characterization with experiments in a way that more fully incorporates data content and is robust enough to treat data with noise and discontinuities.

ACKNOWLEDGEMENTS

This work was supported in part by Sandia National Laboratories. Sandia is a multiprogram laboratory operated by Sandia Corporation, a Lockheed Martin Company, for the United States Department of Energy's National Nuclear Security Administration under Contract DE-AC04-94AL85000.

This work was also supported in part by the Institute for Structural Engineering at Stellenbosch University. Their support is gratefully acknowledged.

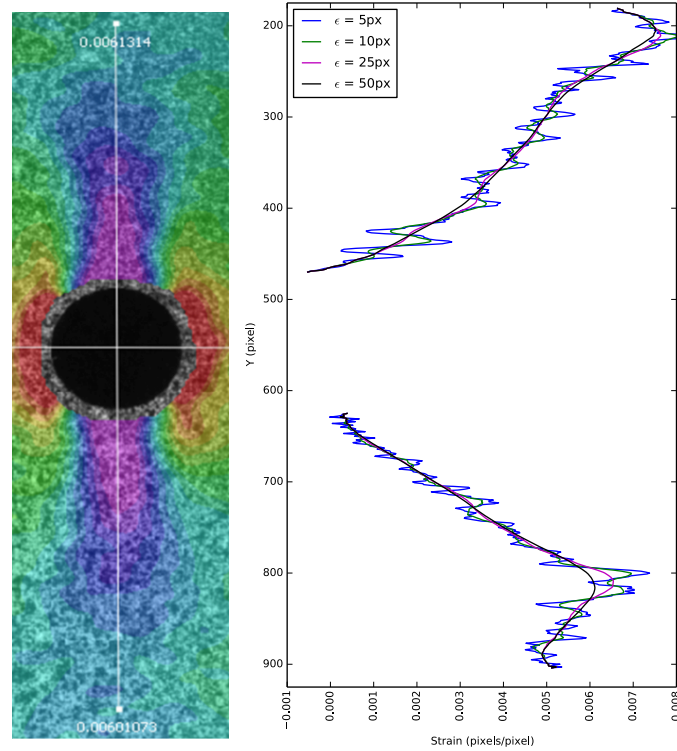


FIGURE 11. Plot of the nonlocal strain for a plate with a hole being loaded in tension for various values of ϵ (the width of the operator's support). The left image shows color contours of the principle strain as calculated using a virtual strain gauge in VIC 2D. Note that increasing ϵ has the effect of filtering high frequency noise in the displacement solution.

REFERENCES

- [1] M. A. Sutton, J. J. Orteu, and H. Schreier. *Image Correlation for Shape, Motion and Deformation Measurements: Basic Concepts, Theory and Applications*. Springer, New York, USA, 2009.
- [2] H.A. Bruck, S. R. McNeill, M. A. Sutton, and W. H. Peters. Digital image correlation using Newton-Raphson method of partial differential correction. *Experimental Mechanics*, 29(3):261–267, 1989.
- [3] F. Hild and S. Roux. Digital Image Correlation: from Displacement Measurement to Identification of Elastic Properties - a Review. *Strain*, 42(2):69–80, 2006.
- [4] T. C. Chu, W. F. Ranson, M. A. Sutton, and W. H. Peters. Applications of Digital-Image-Correlation Techniques to Experimental Mechanics. *Experimental Mechanics*, 25(3):232–244, 1985.
- [5] S. Roux, J. Réthoré, and F. Hild. Digital image correlation and fracture: an advanced technique for estimating stress intensity factors of 2D and 3D cracks. *Journal of Physics D: Applied Physics*, 42(21):1–21, 2009.
- [6] S. R. McNeill, W. H. Peters, and M. A. Sutton. Estimation of stress intensity factor by digital image correlation. *Engineering Fracture Mechanics*, 28(1):101–112, 1987.

- [7] J. Réthoré, A. Gravouil, F. Morestin, and A. Combescure. Estimation of mixed-mode stress intensity factors using digital image correlation and an interaction integral. *International Journal of Fracture*, 132:65–79, 2005.
- [8] J. Réthoré, S. Roux, and F. Hild. From pictures to extended finite elements: extended digital image correlation (X-DIC). *Comptes Rendus Mécanique*, 335(3):131–137, 2007.
- [9] J. Poissant and F. Barthelat. A Novel “Subset Splitting” Procedure for Digital Image Correlation on Discontinuous Displacement Fields. *Experimental Mechanics*, 50:353–364, 2010.
- [10] P. Reu. Introduction to digital image correlation: Best practices and application. *Experimental Techniques*, 36(1):3–4, 2012.
- [11] B. Pan, K. Qian, H. Xie, and A. Asundi. Two-dimensional digital image correlation for in-plane displacement and strain measurement: a review. *Measurement Science & Technology*, 20, 2009.
- [12] S. N. Grama and S. J. Subramanian. Computation of Full-field Strains Using Principal Component Analysis. *Experimental Mechanics*, 54:913–933, 2014.
- [13] Q. Du, M. Gunzburger, R. B. Lehoucq, and K. Zhou. A nonlocal vector calculus, nonlocal volume-constrained problems, and nonlocal balance laws. *Mathematical Models and Methods in Applied Sciences*, 23(3):493–540, 2013.
- [14] M. Gunzburger and R. B. Lehoucq. A nonlocal vector calculus with applications to nonlocal boundary value problems. *Multiscale Modeling & Simulation*, 8:1598–1598, 2010.
- [15] Q. Du, M. Gunzburger, R. B. Lehoucq, and K. Zhou. Analysis and approximation of nonlocal diffusion problems with volume constraints. *SIAM Review*, 54:667–696, 2012.
- [16] Q. Du, M. Gunzburger, R. B. Lehoucq, and K. Zhou. Analysis of the volume-constrained peridynamic Navier equation of linear elasticity. *Journal of Elasticity*, 113:193–217, 2014.
- [17] S. A. Silling, M. Epton, O. Weckner, J. Xu, and E. Askari. Peridynamic States and Constitutive Modeling. *Journal of Elasticity*, 88:151–184, 2007.
- [18] P. Reu, B. Wattrisse, W. Wang, L. Robert, H. Bruck, S. Daly, R. Rodriguez-Vera, and F. Bugarin. Society for Experimental Mechanics: Digital Image Correlation (DIC) Challenge Web page, 2014. <http://www.sem.org/dic-challenge/>.
- [19] X. D. Ke, H. W. Schreier, M. A. Sutton, and Y. Q. Wang. Error Assessment in Stereo-based Deformation Measurements, Part II: Experimental Validation of Uncertainty and Bias Estimates. *Experimental Mechanics*, 51:423–441, 2011.
- [20] J. Blaber and A. Antoniou. Ncorr: Open-source 2D Digital Image Correlation Matlab Software, 2014. <http://www.ncorr.com/>.

RICHARD B. LEHOUCQ, COMPUTATIONAL MATHEMATICS, SANDIA NATIONAL LABORATORIES, P.O. BOX 5800; ALBUQUERQUE, NEW MEXICO 87185. *E-mail address:* `RBLEHOU@SANDIA.GOV`, *Phone:* (505) 845-8929

PHILLIP H. REU, SENSING & IMAGING TECHNOLOGIES, SANDIA NATIONAL LABORATORIES, P.O. BOX 5800; ALBUQUERQUE, NEW MEXICO 87185. *E-mail address:* `PLREU@SANDIA.GOV`, *Phone:* (505) 284-8913

CORRESPONDENCE TO: DANIEL Z. TURNER, MULTISCALE SCIENCE, SANDIA NATIONAL LABORATORIES, P.O. BOX 5800; ALBUQUERQUE, NEW MEXICO 87185. *E-mail address:* `DZTURN@SANDIA.GOV`, *Phone:* (505) 845-7443